Nitrogen abundances of the Be-type stars in 30 Doradus

Monthly Notices of the ROYAL ASTRONOMICAL SOCIETY

MNRAS **527,** 5155–5165 (2024) https://doi.org/10.1093/mnras/stad3537
Advance Access publication 2023 November 16

Nitrogen abundances of the Be-type stars in 30 Doradus

P. L. Dufton,[1]★ N. Langer,[2] D. J. Lennon,[3] F. R. N. Schneider [4,5] C. J. Evans,[6] H. Sana [7] and W. D. Taylor[8]

[1]*Astrophysics Research Centre, School of Mathematics and Physics, Queen's University Belfast, Belfast BT7 1NN, UK*
[2]*Argelander-Institut für Astronomie der Universität Bonn, Auf dem Hügel 71, D-53121 Bonn, Germany*
[3]*Instituto de Astrofísica de Canarias, E-38200 La Laguna, Tenerife, Spain*
[4]*Heidelberger Institut für Theoretische Studien, Schloss-Wolfsbrunnenweg 35, D-69118 Heidelberg, Germany*
[5]*Astronomisches Rechen-Institut, Zentrum für Astronomie der Universität Heidelberg, Mönchhofstr. 12-14, D-69120 Heidelberg, Germany*
[6]*European Space Agency, ESA Office, Space Telescope Science Institute, 3700 San Martin Drive, Baltimore, MD 21218, USA*
[7]*Institut voor Sterrenkunde, Universiteit Leuven, Celestijnenlaan 200 D, B-3001 Leuven, Belgium*
[8]*UK Astronomy Technology Centre, Royal Observatory Edinburgh, Blackford Hill, Edinburgh, EH9 3HJ, UK*

Accepted 2023 November 13. Received 2023 October 13; in original form 2023 July 12

ABSTRACT

A sub-set of the 67 Be-type stars observed in 30 Doradus during the VLT-FLAMES Tarantula Survey (VFTS) campaign have been analysed to estimate atmospheric parameters and chemical compositions, in particular their nitrogen abundance. Reliable results were found for 23 targets comprising the largest Large Magellanic Cloud sample currently available. The nitrogen abundance estimates have been compared with predictions from evolutionary models for rapidly rotating single stars (or non-interacting multiple systems) and for interacting binaries. The observations appear to be incompatible with all the targets having a single star evolutionary history. The results agree better with a binary evolutionary history with at least 30 per cent of the VFTS sample having apparently evolved by this pathway. These conclusions are consistent with a previous analysis of the $v_e \sin i$-estimates for this Be-type sample.

Key words: stars: abundances – stars: emission-line, Be – stars: evolution – stars: rotation – Magellanic Clouds – galaxies: star clusters: individual: Tarantula Nebula.

1 INTRODUCTION

Since their first identification nearly 100 yr ago (Struve 1931), the evolutionary status of Be-type stars has remained uncertain. Observationally they have a circumstellar disc that leads to the emission features in their spectrum and their spectral classification (see e.g. Jaschek & Jaschek 1990). They appear to have systematically larger rotational velocities than normal B-type stars of a similar spectral type (Struve 1931; Zorec et al. 2016). Zorec & Briot (1997) estimated that approximately 17 per cent of Galactic B-type stars were Be-type, with higher estimates having been found in the Large Magellanic Cloud (LMC; 17–20 per cent; Martayan et al. 2006) and the Small Magellanic Cloud (SMC; 26–40 per cent; Martayan et al. 2007). More recently, Schootemeijer et al. (2022) found similar estimates for the Magellanic Clouds, viz. LMC: 22 per cent and SMC: 31 per cent.

Two evolutionary pathways have been suggested to explain the Be-phenomenon. First, that they are single stars (or non-interacting binary systems), that have rotational velocities close to their critical velocities. This could arise from either a high initial rotational velocity although some observational studies of stellar rotation rates (Zorec et al. 2016; Bodensteiner, Shenar & Sana 2020; Dufton et al. 2022) do not support such high values. Alternatively, it could arise from the decrease in the critical velocity as a B-type star evolves from the zero-age main sequence. Recently, Hastings, Wang & Langer (2020) have discussed this scenario in detail and concluded that it required that the Be-type star rotated at ∼70–80 per cent of its critical velocity. Additionally, their population synthesis for the SMC cluster, NGC 330 was inconsistent with the observation of Be-type stars almost two magnitudes below the main-sequence turn-off (Milone et al. 2018).

A second evolutionary pathway requires that Be-type stars form within a binary (or multiple) system and subsequent interactions lead to the Be-type phenomena (see e.g. van den Heuvel & Rappaport 1987; Pols et al. 1991; De Mink et al. 2013; Rivinius, Carciofi & Martayan 2013; Shao & Li 2014, 2020; Hastings et al. 2021). Now, the observed Be-type star was originally the less-massive component but has accreted mass and angular momentum from the primary, which may become a supernova (see e.g. Hastings et al. 2021), a stripped He-type star (see e.g. Shao & Li 2021) or a white-dwarf. The mass transfer leads to the original secondary rotating rapidly, which in turn leads to a Be-type classification. This pathway would appear to be responsible for the approximately 100 known OBe-type/X-ray binaries (Reig 2011). Additionally binaries have been identified containing Be-type stars with a white-dwarf (Kennea et al. 2021) or with sdO-type companions (see e.g. Thaller et al. 1995; Wang et al. 2021).

★ E-mail: P.Dufton@qub.ac.uk

Recent observational studies have found relatively few Be-type stars that have been identified as binaries (Evans et al. 2015; Bodensteiner, Shenar & Sana 2020; Villaseñor et al. 2021). However, this may not be inconsistent with the binary-formation hypothesis as the expected radial velocity variations of the now significantly more massive Be-type star would be small and therefore might not be detected even with multiple observations at different epochs (see e.g. Sana et al. 2013; Dunstall et al. 2015). Indeed, Bodensteiner, Shenar & Sana (2020) suggested that the absence of Galactic binary systems consisting of a Be-type star and a normal massive B-type star supported the evolutionary pathway involving an interacting binary system.

A potential diagnostic for distinguishing between these two pathways is the surface nitrogen abundance of Be-type stars. For example previous studies have found that many Be-type stars have relatively small nitrogen enrichment, with less than one third of the Galactic Be-type stars in the analysis of Ahmed & Sigut (2017) having nitrogen enhancements >0.2 dex. Additionally, Dunstall et al. (2011) found similar nitrogen abundances in their Magellanic Cloud samples of both B-type and Be-type stars, whilst comparison of the latter with the population synthesis predictions of Brott et al. (2011b) were inconsistent with the strong rotational mixing assumed to be present in stars rotating at near critical velocities.

Here, we estimate stellar parameters and element abundances for Be-type stars in 30 Doradus in the Large Magellanic Cloud. The VLT-FLAMES Tarantula Survey (VFTS) obtained multi-epoch optical spectroscopy of over 800 massive stars in the 30 Doradus region (Evans et al. 2011), including 73 targets classified as Be-type by Evans et al. (2015). The only selection criterion was a magnitude cut-off in order to provide sufficient signal-to-noise (S/N) ratios in the spectroscopy. As such they provide a relatively unbiased Be-type sample, which we analyse to estimate their chemical composition, and in particular their nitrogen abundances. Useful results could only be obtained for approximately one third of the sample but these are sufficient for a comparison with the predictions of the two evolutionary pathways outlined above.

2 OBSERVATIONS

The VFTS spectroscopy was obtained using the MEDUSA mode of the FLAMES instrument (Pasquini et al. 2002) on the ESO Very Large Telescope and has been discussed in detail by Evans et al. (2011).MEDUSA uses fibres to simultaneously 'feed' the light from over 130 sky positions to the Giraffe spectrograph. Nine fibre configurations (designated fields 'A' to 'I' with near-identical field centres) were observed in the 30 Doradus region, sampling different clusters and the local field population. Three standard Giraffe grating settings were used viz. LR02 (wavelength range from 3960 to 4564 Å at a spectral resolving power of R ∼ 7000), LR03 (4499–5071 Å, R ∼ 85 000), and HR15N (6442–6817 Å, R ∼ 16 000). Evans et al. (2015) identified Be-type characteristics from stellar Hα emission in their HR15N spectroscopy and subsequently, Dufton et al. (2022) were able to estimate atmospheric parameters and projected rotational velocities for 67 of these targets. Details of the target selection, observations, and initial data reduction have been given in Evans et al. (2011).[1] Subsequent data reduction has been discussed in Dufton et al. (2022), where details can also be found of SB1 binarity and the possibility of flux contamination from spatial close companions. For the latter, only #283 may be affected with two additional stars having comparable *I*-band magnitude lying at ∼0.5 arcsec.

For both the LR02 and LR03 spectroscopy,[2] all useable exposures were combined using either a median or weighted σ-clipping algorithm. The final spectra from the different methods were normally indistinguishable. The full wavelength range for each wavelength setting could usually be normalized using a single, low-order polynomial. However, for some features (e.g. the Balmer series), the combined spectra around individual (or groups of) lines were normalized.

In the model atmosphere analysis, equivalent widths were generally used for the metal lines, with profiles being considered for the broader H I and He II lines. For the former, rotationally broadened profiles (with the $v_e \sin i$-estimates from Dufton et al. 2022), together with a low-order polynomial to represent the continuum were fitted to the observed spectra leading to formal errors in the equivalent width estimates of typically 10–20 per cent. The fits were generally convincing which is consistent with the intrinsic and instrumental broadening being minor contributors in these generally broad-lined spectra.

For some spectra, the N II line at 3995 Å could not be seen; in these cases we have set upper limits on its equivalent width. Our approach was to measure the equivalent width of the weakest metal lines that were observable in the corresponding LR02 spectrum. We emphasize that this will lead to conservative estimates both for the upper limits of equivalent widths and for the corresponding element abundances.

3 MODEL ATMOSPHERE ANALYSIS

The nature of Be-stellar spectra makes quantitative analysis of their spectra more difficult than for normal B-type stars (see e.g. Dunstall et al. 2011; Ahmed & Sigut 2017; Dufton et al. 2022). Indeed at near critical rotational velocities, the conventional model atmosphere assumption of plane-parallel (or spherical) geometry breaks down. Then as discussed by Zorec et al. (2016), atmospheric parameters estimated assuming such geometries represent some average over the spatially varying photospheric conditions. Additionally, the observed spectrum may be contaminated by emission from a circumstellar disc (Rivinius, Carciofi & Martayan 2013; Ahmed & Sigut 2017). Here, we have adopted a relatively simple approach and used non-LTE model atmospheres that assume a plane-parallel geometry, hydrostatic, and radiative equilibrium. In Section 4, we discuss the reliability of these results.

We have employed model-atmosphere grids calculated with the TLUSTY and SYNSPEC codes (Hubeny 1988; Hubeny & Lanz 1995; Hubeny, Heap & Lanz 1998; Lanz & Hubeny 2007). They cover a range of effective temperature, 10 000 K $\leq T_{\rm eff} \leq$ 35 000 K in steps of typically 1500 K. Logarithmic gravities (in cm s^{-2}) range from 4.5 dex down to the Eddington limit in steps of 0.25 dex, and microturbulences are from 0 to 30 km s^{-1} in steps of 5 km s^{-1}. As discussed in Ryans et al. (2003) and Dufton et al. (2005), equivalent widths and line profiles interpolated within these grids are in good agreement with those calculated explicitly at the relevant atmospheric parameters. Grids have been calculated for a range of metallicities with that for an LMC metallicity being adopted here. The analysis assumes a normal helium to hydrogen ratio (0.1 by

[1]Additional LR02 spectroscopy from Villaseñor et al. (2021) for four SB1 candidates has also been used with the initial reduction procedures following those for the VFTS data.

[2]The DR2.2 pipeline reduction was adopted and the spectra are available at http://www.roe.ac.uk/∼cje/tarantula/spectra.

Table 1. Atmospheric parameters, disc contributions, and abundances estimates for the analysed VFTS Be-type stars. Stars marked with asterisks have been classified as spectroscopic binaries. Also listed are the methods used to estimate the effective temperature, spectral types (Evans et al. 2015), and projected rotational velocities, $v_e \sin i$ (Dufton et al. 2022).

VFTS	ST	$v_e \sin i$ km s^{-1}	f_c	T_{eff} K	Method	log g cm s^{-2}	$\Delta\epsilon_C$	$\Delta\epsilon_N$	$\Delta\epsilon_O$	$\Delta\epsilon_{Mg}$	$\Delta\epsilon_{Si}$
034	B1.5Ve	174	0	25 000	He II	4.1	0.21	≤0.2	0.13	0.36	−0.01
101	B0.7: Vne	354	13	28 000	ST	4.1	–	≤1.2	–	–	−0.01
135*	B1: V-IIIne	299	0	25 500	ST	3.8	–	0.98	–	–	0.25
152	B2 IIIe	48	31	20 000	Si II	3.4	−0.13	0.31	−0.01	−0.19	0.00
164	B2: V-IIIe +	190	0	23 100	ST	3.7	0.12	≤0.3	–	0.02	0.01
194	B2 V-IIIe +	217	0	23 100	ST	3.6	0.16	≤0.3	0.26	−0.02	0.07
196	B2 IIIe +	200	26	21 700	ST	3.5	0.07	≤0.5	–	−0.09	0.01
213*	B2 III:e	145	5	21 700	ST	3.5	−0.04	−0.03	−0.04	−0.07	0.00
237	B1-1.5 V-IVe	96	4	24 000	Si IV	3.8	0.15	0.32	−0.15	0.03	0.01
268	B1.5 Ve +	199	0	25 700	ST	3.9	−0.14	0.94	–	–	0.02
283	B1.5 V-III(n)e	279	0	24 300	ST	3.7	−0.06	0.55	0.02	−0.08	0.09
293	B2 III-II(n)e	110	18	21 000	ST	3.4	0.13	−0.03	−0.18	−0.12	0.01
322	B1.5-2 Ve +	166	10	25 100	ST	3.8	0.28	≤0.6	–	–	0.00
395	B1:e	66	26	24 500	Si IV	3.5	−0.21	≤0.1	0.05	0.00	0.00
683	B2 Ve	290	5	24 500	ST	3.9	0.15	≤0.4	–	0.05	−0.01
697*	B1-2 Ve	121	22	25 000	He II	4.0	0.26	0.62	0.07	−0.13	−0.01
738	B0.5 IIIe +	190	0	27 500	He II	3.5	−0.16	0.33	0.19	–	0.11
756	B0.5 IIIe +	143	0	23 500	He II	3.2	−0.07	0.73	−0.10	–	0.07
825	B1.5-2 V-IIIe	270	0	23 700	ST	3.4	0.12	≤0.6	–	–	0.16
835	B1 Ve	49	12	25 500	Si IV	4.2	0.13	0.30	0.04	0.02	0.00
847*	B0.7-1 IIIne	258	0	24 800	ST	3.5	–	0.56	–	–	0.18
848	B1.5 IIIe +	150	29	23 000	ST	3.4	0.23	≤0.3	−0.08	–	0.01
874*	B1.5 IIIe +	67	27	22 950	ST	3.9	−0.13	−0.25	−0.16	–	−0.01
Mean	–	–	–	–	–	–	0.05 ± 0.16	–	0.00 ± 0.13	−0.02 ± 0.13	–

number of atoms) and, as discussed by Dufton et al. (2018), the targets with large nitrogen enhancements might also be helium-rich. However, for the LMC evolutionary models, Brott et al. (2011a) found that even for a nitrogen enhancement of 1.0 dex (which is larger than the enhancements observed in our sample – see Table 1), the change in the helium abundance was typically only 0.03 dex. Hence, our assumption of a normal helium abundance is unlikely to be a significant source of error.

Initially we adopted the atmospheric parameters of Dufton et al. (2022), which were estimated using these grids. Effective temperature estimates were from either the silicon ionization equilibrium or the He II spectrum. Where these were not available, the calibration of effective temperature against spectral-type for the LMC of Trundle et al. (2007), which was derived from analyses using the same model atmosphere grids as adopted here, was used. Surface gravities (in cm s^{-2}) had been found from fitting the observed H γ and H δ profiles. Microturbulent velocities, v_t, were not estimated by Dufton et al. (2022) but could in theory be estimated from the relative strength of lines within the Si III triplet near 4560 Å. However, all three lines were not always available (see Appendix A), and hence we have instead adopted zero for all our targets. We discuss the implications of this choice in Section 4.1.

These initial estimates assumed that any spectral contribution from a circumstellar disc was negligible. Previously, Dunstall et al. (2011) found significant contributions for Be-type stars located in the Magellanic Clouds. To attempt to estimate such a contribution we have adopted their approach, which assumed the contribution from the circumstellar disc was a featureless continuum, that was a constant fraction of the stellar continuum over the spectral range considered.

The methodology takes the silicon abundance estimates deduced from the Si III triplet and compares them to a baseline LMC abundances. The latter is assumed to be 7.2 dex based on the analysis of LMC B-type stars using observational data obtained with the same instrumentation and analysed using the same model atmospheres (Hunter et al. 2007, 2009; Trundle et al. 2007). Hence, it should be appropriate for such a comparison as any systematic errors should be minimized. Additionally, this baseline abundance has been found to be consistent with the analysis of VFTS B-type spectra (Garland et al. 2017; Dufton et al. 2018).

For each target, the difference (δSi) in the estimated silicon abundance to the baseline abundance is used to estimate the fractional contribution (f_c) of the disc continuum. The equivalent widths of all metal lines are then scaled by the reciprocal of (1-f_c) and used to re-estimate the effective temperature for stars using the silicon ionization balance. For stars with temperatures estimated using the He II spectrum, the line profiles were corrected by subtracting the estimated fractional contribution and re-normalizing the feature.[3] A similar procedure is applied to the observed Balmer lines and the surface gravity re-estimated. With these new atmospheric parameters, silicon abundances are re-estimated and an iteration procedure repeated until the absolute value of δSi was <0.02 dex. This procedure normally increased both the effective temperature and logarithmic gravity estimates by up to 1000 K and 0.3 dex, respectively.

For six targets, the silicon abundance was larger than the baseline abundance even for no disc contribution. In three cases, the difference was <0.1 dex and could be due to observational errors. For the other three cases, the discrepancy may arise from the assumption of zero microturbulence with a value of $v_t \gtrsim 2$ km s^{-1} being sufficient to

[3]Effective temperatures estimated from the spectral type remained unchanged.

Table 2. Atmospheric parameters, disc contributions, and abundances estimates for three VFTS Be-type stars for microturbulences of 0 and 5 km s^{-1}.

VFTS	$T_{\rm eff}$ K	$\log g$ cm s^{-2}	$v_{\rm t}$ km s^{-1}	$f_{\rm c}$	$\Delta\epsilon_{\rm C}$	$\Delta\epsilon_{\rm N}$	$\Delta\epsilon_{\rm O}$	$\Delta\epsilon_{\rm Mg}$	$\Delta\epsilon_{\rm Si}$
213	21 700	3.5	0	5	− 0.04	− 0.03	− 0.04	− 0.07	0.00
213	21 700	3.8	5	26	0.12	0.11	0.21	− 0.04	0.00
237	24 000	3.8	0	4	0.15	0.32	− 0.15	0.03	0.01
237	25 500	4.2	5	25	0.44	0.49	− 0.08	0.22	0.00
738	27 500	3.4	0	0	− 0.16	0.33	0.19	–	0.11
738	28 500	3.7	5	14	0.04	0.48	0.19	–	0.00

achieve a baseline abundance – see Appendix A for more details. This illustrates the sensitivity of our results to the adopted microturbulence which is discussed further in Section 4.1.

Using these iterated atmospheric parameters and the scaled equivalent widths, abundance estimates (or upper limits) were obtained for carbon, nitrogen, oxygen, and magnesium for 23 Be-type stars in the VFTS sample, being approximately one third of our sample. For the remaining targets, their Si III spectrum could not be observed due to their large projected rotational velocities. In turn, this precluded an estimate of the disc contribution, $f_{\rm c}$. Atmospheric parameters, disc contributions, and element abundances are summarized in Table 1, together with spectral types (Evans et al. 2015) and projected rotational velocities (Dufton et al. 2022). The element abundances are shown relative to baseline LMC abundances, which as for the silicon abundance were taken from the analyses of Hunter et al. (2007, 2009)[4] and Trundle et al. (2007).

4 RELIABILITY OF THE MODEL ATMOSPHERE ANALYSIS

Below, we consider possible sources of uncertainty in the estimates from the model atmosphere analysis considered in Section 3. In particular, we attempt to assess the reliability of the nitrogen abundance estimates, which are the principal focus of this investigation.

4.1 Microturbulent velocity

The model atmosphere analysis assumed a zero microturbulence ($v_{\rm t}$), although there was evidence that this might be higher in some of our targets as discussed in Appendix A. We have therefore, repeated the analysis for three targets (#213, 237, and 738) adopting a microturbulence, $v_{\rm t} = 5$ km s^{-1}. These stars were chosen as they utilized different effective temperature estimators and covered a range of atmospheric parameters. The results of the analyses are summarized in Table 2, with the results for zero microturbulence being taken directly from Table 1. Below, we discuss each star separately:

#213: The effective temperature was estimated from the spectral type and hence is unaffected by the choice of microturbulence. However, the disc contribution is significantly larger for the increased microturbulence and now contributes approximately one quarter of the flux. In turn, the scaled Balmer line profiles lead to an increase in the surface gravity of 0.3 dex. All the element abundance estimates have increased, principally due to the increase in the adopted equivalent widths. However, the increases range from between 0.03 and 0.25 dex, reflecting different sensitivities of the theoretical line strengths to the adopted gravity. For example at this effective temperature, the predicted O II spectrum weakens as the gravity is increased. This coupled with an increase in the observational line strengths leads to a relatively large increase of 0.25 dex in the oxygen abundance. By contrast, the predicted strength of the Mg II doublet at 4481 Å increases with increasing gravity leading to an increase of only 0.03 dex in the estimated abundance. The theoretical N II spectrum is relatively insensitive to the adopted gravity and the increase in the abundance estimate of 0.14 dex reflects the increase in observational line strength partially mitigated by the larger theoretical line strengths for an increased microturbulence.

#237: The effective temperature was estimated from the silicon ionization equilibrium and is hence directly affected by the change in microturbulence and indirectly by the increases in the disc contribution, $f_{\rm c}$, and the gravity. This target shows the largest change in atmospheric parameters with increases of 1500 K in $T_{\rm eff}$ and 0.4 dex in gravity. Additionally, the estimated flux contribution from the disc is increased to one third of that of the total flux. Changes in the abundance estimates range from 0.07 to 0.29 dex, again reflecting the different sensitivities of their predicted spectra to the atmospheric parameters, with that for nitrogen being 0.17 dex.

#738: The effective temperature was estimated from the He II lines, whose theoretical line strengths are insensitive to the adopted microturbulence. However, the $T_{\rm eff}$ -estimate is affected by both the increased gravity and disc flux contribution. The oxygen abundance estimate is unchanged, whilst those for carbon and nitrogen are increased by 0.20 and 0.15 dex, respectively, again reflecting different sensitivities of their predicted spectra to the atmospheric parameters.

These investigation have led to similar increases in the nitrogen abundance estimates for all three stars. For the range of atmospheric parameters considered here, the theoretical N II spectrum is close to its greatest strength and hence relatively insensitive to changes in these parameters. Consequently, the increase in the nitrogen abundance estimates mainly reflects the increase in observational line strengths. We conclude that the nitrogen abundances may have been underestimated by the adoption of zero microturbulence, with an increase to 5 km s^{-1} increasing the nitrogen abundance estimate by typically 0.15 dex.

5 STOCHASTIC UNCERTAINTIES

Stochastic uncertainties will arise from limitations in the observational data affecting the atmospheric parameters. For the effective temperature estimates, a change of 1000 K significantly worsened the agreement between theory and observation for the He II profiles as can be seen in Fig. 1. For the estimates from the silicon ionization equilibrium, a similar change in effective temperature led to a typical difference of 0.3–0.4 dex in the two silicon abundance estimates. To remove this would require changes in the equivalent widths of 30

[4]The baseline abundances are $\epsilon_{\rm C} = 7.75$, $\epsilon_{\rm N} = 6.90$, $\epsilon_{\rm O} = 8.35$, and $\epsilon_{\rm Mg} = 7.05$ dex.

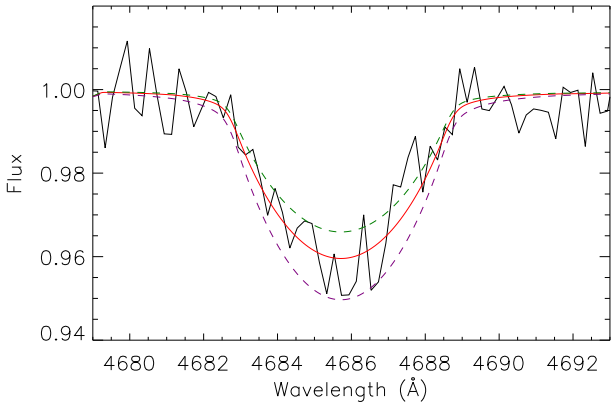

Figure 1. Observed (solid black line) and theoretical (solid line) profiles for the He II line at 4686 Å in #738. Also shown are theoretical profiles with the effective temperature decreased and increased by 1000 K (dotted green and purple lines, respectively).

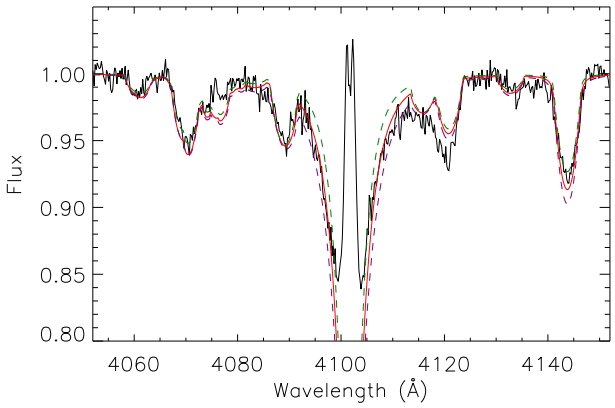

Figure 2. Observed (solid black line) and theoretical (solid line) profiles for the Balmer line at 4102 Å in #738. Also shown are theoretical profiles with the gravity decreased and increased by 0.2 dex (dotted green and purple lines, respectively).

per cent or more, which can be compared with the typical formal errors of 10–20 per cent discussed in Section 2.

The uncertainty in the effective temperature estimates from the spectral types will be larger. Dufton et al. (2019) estimated an uncertainty of ±1500 K for targets in the SMC cluster, NGC 346 but their sample was predominantly normal B-type stars with only 15 per cent classified as Be-type. Here, we can compare the nine estimates from the helium or silicon spectra with those implied by the spectral type. The latter range from 1800 K higher to 1000 K lower, with a mean difference of 740 ± 980 K. Hence, there is some evidence that the effective temperature estimates from the spectral type may be higher and we note that the calibration that we used was developed using normal B-type stars, with relatively narrow absorption spectra. We have adopted a conservative uncertainty in the effective temperature of all our targets of ±2000 K.

The stochastic uncertainty in the gravity estimate arises from the finite S/N of the spectroscopy and the difficulty of normalizing the spectroscopy especially when there are nearby metal and helium lines. This is illustrated in Fig. 2 for the relatively hot target #738. Its H δ line lies close to strong oxygen lines at 4070–4090 Å and helium lines at 4121 and 4143 Å, and the normalization in the red wing of H δ may be incorrect due to helium lines. However the gravity appears to be constrained to ±0.2 dex. Although the fits to the cooler targets

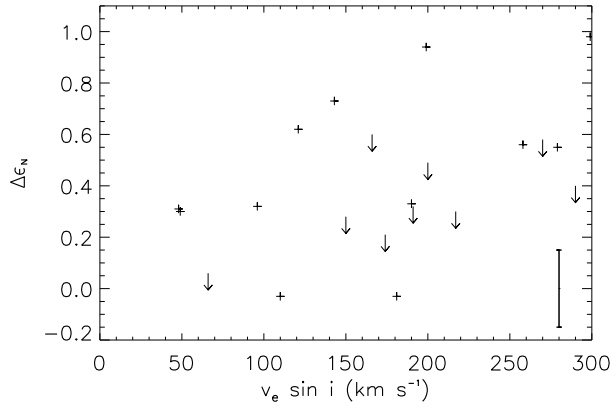

Figure 3. Nitrogen abundance estimates (and upper limits) relative to the adopted LMC baseline value ($\Delta\epsilon_N$) plotted against the v_e sin i-estimates. Also shown is a typical error bar in the abundance estimates.

are generally less affected by blending, we have again adopted a conservative uncertainty in gravity of ±0.2 dex.

Adopting the above uncertainties in the atmospheric parameters, we can estimate the uncertainties in the nitrogen abundance estimate. The median values of our effective temperature and gravity estimates are 24 300 K and 3.7 dex, respectively. Changing the former by the estimated uncertainty (±2000 K) changes the abundance estimates by typically 0.05–0.10 dex depending on the strength of the nitrogen line. The changes caused by the gravity uncertainty (±0.2 dex) are smaller and always <0.05 dex. These relatively small values arise from the N II spectrum being close to its maximum strength at the median atmospheric parameters.

We can also use the abundance estimates for the other elements to assess uncertainties. At the bottom of Table 1, we list the mean and standard deviations for the abundance estimates of these elements.[5] The mean values are all close to zero, consistent with the abundances for these elements having not been affected by the star's evolution. The standard deviations provide an estimate of the typical element uncertainty and are all ∼0.15 dex, which is consistent with the uncertainties in the nitrogen abundances discussed above. Hence, we adopt a *stochastic* uncertainty in our abundance estimates of ∼0.15 dex.

6 NITROGEN ABUNDANCE ESTIMATES

The nitrogen abundance estimates are summarized in Table 1 and are relative to an adopted LMC baseline nitrogen abundance, $\epsilon_N = 6.9$ dex. This is based on analyses of B-type spectra (Hunter et al. 2007; Trundle et al. 2007) and as discussed by Dufton et al. (2018) is in excellent agreement with that found from H II regions (Kurt & Dufour 1998; Garnett 1999; 6.92 and 6.90 dex, respectively).

The nitrogen abundance estimates are plotted in Fig. 3 and range from the adopted LMC baseline abundance to an enhancement of nearly 1.0 dex. There is no obvious correlation of these estimates with the corresponding v_e sin i-estimates as might be expected if significant rotational mixing had occurred. In general, the enhancements are modest with a median value of 0.33 dex. As discussed in Section 4.1, the adoption of zero microturbulence may have led to an underestimate of these enhancement, which for $v_t = 5$ km s^{-1} would amount to typically 0.15 dex.

[5]No statistics are given for silicon as its abundance was used to constrain the disc flux contribution.

Nitrogen abundances have been previously estimated by Ahmed & Sigut (2017) for a sample of 26 Galactic Be-type stars and Dunstall et al. (2011) for a sample of 31 Be-type stars in the Magellanic Clouds. Ahmed & Sigut (2017) undertook a comprehensive analysis which included corrections for gravity darkening and disc contamination. Their adopted nitrogen abundances range from approximately 7.24 to 8.52 dex (see their fig. 25) and they commented that 'a significant number of Be stars, about 10 out of 26, have decidedly sub-solar nitrogen abundances'. They discussed several explanations for this including uncertainties in their theoretical models and the possibility of unseen binary companions. Only one third of their sample showed nitrogen enhancements and these were generally small.

The analysis of Dunstall et al. (2011) used a methodology similar to that adopted here. For their 15 LMC targets they found nitrogen enhancements (with one upper limit) in the range 0.1–1.1 dex. Their median enhancement was 0.35 dex, which is very similar to that found for our current LMC targets. For their 16 SMC targets, it was only possible to estimate nitrogen abundances for half the sample. This reflects the low baseline nitrogen abundance, ∼6.5 dex, of the SMC, which would lead to an intrinsically weak N II spectrum, when the nitrogen enhancement was small. Hence, it is not possible to deduce a median enhancement although enhancements (and upper limits) range from 0.2 to 1.3 dex.

Dunstall et al. (2011) noted that the nitrogen abundances of Magellanic Cloud normal B-type and their Be-type stars were similar. Additionally, Ahmed & Sigut (2017) found that the average nitrogen abundances for their Galactic B-type and Be-type star samples coincided with the solar abundance, although the dispersion was larger in the Be-type star sample. We can compare our estimates with those found for VFTS B-type stars by Dufton et al. (2018). Median enhancements for the two samples were very similar, 0.30 (B-type) and 0.33 dex (Be-type), as were the range of nirogen enhancements, ∼0.0–1.1 dex. This is surprising as the sample of Dufton et al. (2018) was limited to VFTS B-type targets with $v_e \sin i$-estimates of $<80\,\mathrm{km\,s^{-1}}$. As such it should be biased towards targets with small rotational velocities and correspondingly small degrees of rotational mixing.

In Section 6.1, we estimate stellar masses on the assumption that our targets are evolving as a single star or a non-interacting binary. For the 13 targets with nitrogen abundance estimates (rather than upper limits), we find some evidence for greater nitrogen enhancements in our more massive targets, as shown in Fig. 4. However as can be seen from the figure, the uncertainties in the mass estimates are large. Also, it is possible that this sample may be biased. For example the more massive stars typically have larger effective temperatures and hence an intrinsically weaker N II spectrum. In turn this would only allow nitrogen abundance estimates for those hotter targets with large enhancements.

Both Ahmed & Sigut (2017) and Dunstall et al. (2011) emphasize the challenges of the quantitative analysis of Be-type spectra and we would endorse these comments. However, these two analyses and the one presented here, all imply that nitrogen enhancements in Be-type stars are generally modest and there is no evidence for enhanced rotational mixing in Be-type stars.

Below we discuss our nitrogen abundance estimates in the context of current evolutionary models for the formation of Be-type stars. These fall into two main categories, viz. that Be-type stars have evolved either as single stars (Struve 1931; Rivinius, Carciofi & Martayan 2013; Hastings, Wang & Langer 2020) or as multiple system with mass transfer (Pols et al. 1991; De Mink et al. 2013; Shao & Li 2014, 2020; Langer et al. 2020b; Hastings et al. 2021).

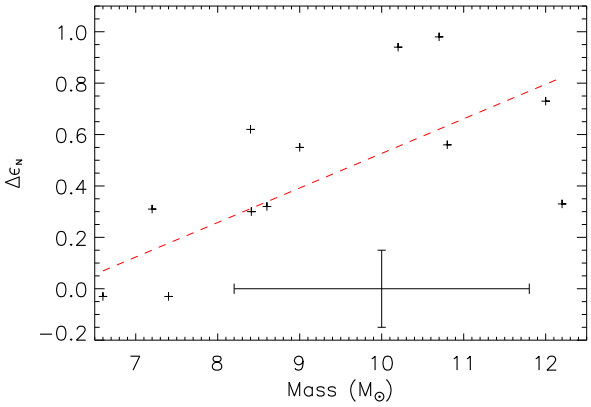

Figure 4. Nitrogen abundance estimates relative to the adopted LMC baseline value ($\Delta\epsilon_N$) plotted against the stellar mass estimates. Also shown are typical error bars in the mass and abundance estimates and a linear least-squares fit to the data.

The former (henceforth designated 'single') could include binary systems, where there have been no significant interaction between the components, whilst the latter (henceforth designated 'binary') could apply to targets that are no longer binaries.

The Be-type phenomenon would appear to be transient with, e.g. γ Cas exhibiting Balmer line emission epochs (see e.g. Doazan et al. 1983; Telting & Kaper 1994). For our VFTS sample, Dufton et al. (2022) estimated that there were more apparently single B-type stars than Be-type stars with rotational velocities >60 per cent of their critical rotational velocity. Unfortunately, statistics for the duration of the Be-type and quiescent phases are not available and hence it is not possible to estimate the number of rapidly rotating B-type stars that are quiescent Be-type. Hence, although our Be-type sample may be incomplete, we would not expect this to lead to any systematic biases that would affect the following discussion.

6.1 Single star evolution

The models of Brott et al. (2011a) can be used to investigate the implications of our nitrogen enrichments being due to single star (or non-interacting binary) evolution. Adopting the median nitrogen enhancement, we have estimated the equatorial rotational velocity and its ratio, γ_e, to the critical velocity. In Fig. 5, these γ_e-estimates are shown as a function of mass for two logarithmic gravities, 3.5 and 4.0 dex. The mass range was chosen to cover the estimates for our sample as discussed below. Also shown are loci assuming a median nitrogen enhancement increased by 0.15 to 0.48 dex, to allow for uncertainties in the microturbulent velocity discussed in Section 4.1. For our median stellar mass of 8.8 $M_\odot$, these would imply, γ_e-values of 0.42–0.46 and 0.50–0.54, respectively. Hence, the modest nitrogen enhancement requires that the majority of Be-type stars are *not* rotating at near critical velocities, as is often assumed (see e.g. Rivinius, Carciofi & Martayan 2013; Bastian et al. 2017).

We have also investigated our sample using BONNSAI,[6] which uses a Bayesian methodology and the grids of models of Brott et al. (2011a) to investigate the evolutionary status of a given star on the assumption that it is undergoing normal single star evolution (see Schneider et al. 2014, for details). As independent prior functions, we adopted the LMC metallicity grid of models, a Salpeter (1955)

[6]The BONNSAI web-service is available at www.astro.uni-bonn.de/stars/bonnsai.

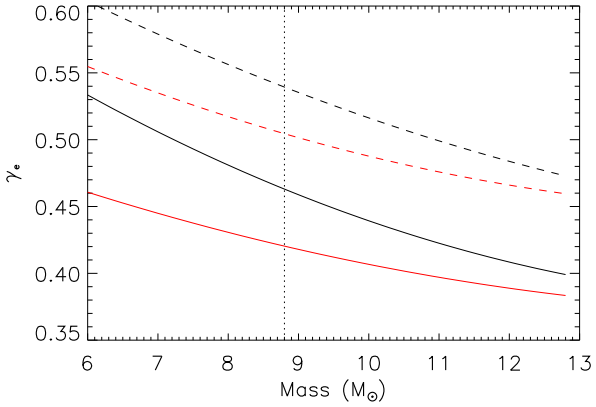

Figure 5. Loci of γ_e-values estimated from single stellar evolutionary models for nitrogen enrichments of 0.33 dex and for values of $\log g$ of 4.0 (solid black line) and 3.5 dex (solid red line). Analogous loci are also shown for an nitrogen enhancement of 0.48 as dotted lines.

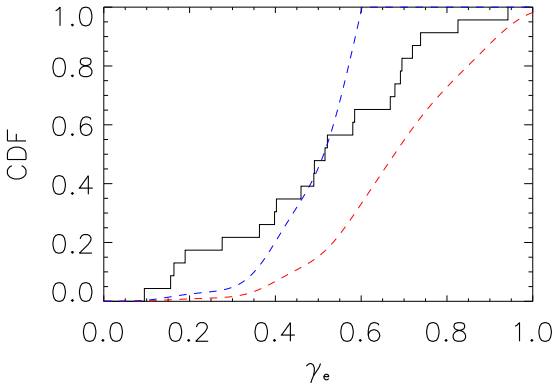

Figure 6. Cumulative distribution function for γ_e-values estimated from the Bonnsai predictions (solid black line) for the 23 targets summarized in Table 1. Also shown are CDFs deduced from the $v_e \sin i$-estimates (Dufton et al. 2022) for the complete VFTS Be-type sample (dotted red line) and for a one third sub-set with the lowest γ_e-values (dotted blue line).

initial mass function, an initial uniform rotational velocity, a random orientation of spin axes, and a uniform age distribution. The estimates of effective temperature, gravity, and nitrogen abundance (taken from Table 1) were adopted, together with the $v_e \sin i$-estimates of Dufton et al. (2022). The uncertainties discussed in Section 5 were used for the first three quantities and assumed to follow a normal distribution, apart from the cases where the nitrogen abundance estimate was an upper limit. The uncertainties in the $v_e \sin i$-estimates were taken from Dufton et al. (2022) on a star-by-star basis and again were assumed to follow a normal distribution. The solution yielded mass estimates ranging from 6.6 to 12.2 $M_\odot$ with a median value of 8.8 $M_\odot$, consistent with that adopted in Fig. 5. The 1 σ-uncertainties in the mass estimates ranged from 16 to 28 per cent with a median of 21 per cent.

The implied γ_e-estimates range from 0.10 to 0.94 with a median value of 0.52, in good agreement with the ranges inferred from Fig. 5. Solutions could not be obtained for four targets (#194, 213, 825, and 848), all of which exhibit relatively low gravities and relatively high $v_e \sin i$-estimates, but small nitrogen enrichment. The targets appear to have evolved from the main sequence and should have undergone significant rotational mixing but this is incompatible with the estimated nitrogen abundance or upper limit. Increasing the nitrogen abundance estimates by 0.15 dex to allow for possible uncertainties associated with the adopted microturbulence (see Section 4.1) lead to possible solutions except for #194.

Inspection of the individual solutions show that the differences in the BONNSAI predicted nitrogen abundances compared to those in Table 1 have a mean of -0.03 ± 0.28 dex. However, the atmospheric parameters predicted by BONNSAI are systematically offset being 1100 ± 200 K lower for $T_{\rm eff}$ and 0.20 ± 0.10 dex higher for $\log g$. The latter would place the BONNSAI solutions nearer to the main sequence thereby reducing the degree of nitrogen enrichment. Inspection of the grid of models of Brott et al. (2011a) shows that decreasing the effective temperature would also decrease the nitrogen enhancement at a given rotational velocity.

The angles of inclination (i) can also be inferred from the observed $v_e \sin i$-estimates and the BONNSAI predictions for the projected rotational velocity. These imply a median value of $\sin i$ of 0.97, with an average value of 0.91. These are both higher than those expected from a random distribution of rotational axes that would imply 0.87 and 0.78, respectively (Gray 2005). Hence, the BONNSAI solutions appear to be seeking smaller rotational velocities than would be implied by a random inclination of axes, in order to reduce the predicted nitrogen enhancement.

The median γ_e-value implied by our nitrogen abundance estimates and a single star evolutionary history is $\sim$0.5, significantly smaller than the median value of $\sim$0.68 found by Dufton et al. (2022) from de-convolution of the $v_e \sin i$-estimates. However, the latter was for a sample of 69 VFTS Be-type stars and here it has only been possible to obtain nitrogen abundance for 23 of these targets. As the identification of weak metal lines is difficult for targets with large $v_e \sin i$-values, our sample may be biased to targets with low γ_e-values. To investigate the magnitude of this bias, we can make an *extreme* assumption that our sample consists of the targets with the lowest one third of γ_e-values in the distribution found by Dufton et al. (2022) – these would then have a median γ_e-value of 0.51 in good agreement with the estimate deduced from the nitrogen abundance estimates, assuming a single star evolutionary history.

In Fig. 6, the cumulative distribution function (CDF) is shown for the γ_e-values implied by the BONNSAI simulations. Also shown are CDFs deduced for the complete VFTS Be-type sample (Dufton et al. 2022, dotted red line) and for a one third sub-set with the lowest γ_e-values (dotted blue line). The agreement between the BONNSAI simulations and CDF for the complete sample is poor with the latter being biased towards larger γ_e-values; this is consistent with their medians as discussed above. The agreement with the CDF for a one third sub-set with the lowest γ_e-values is also poor with the predictions having a lack of targets at both low and high γ_e-values. The latter is a consequence of the choice of the lowest one third of γ_e-values in the distribution found by Dufton et al. (2022); allowing some such targets would improve the agreement at large γ_e-values. However, the disagreement at low γ_e-values reflect the lack of targets with $\gamma_e \lesssim 0.4$ in the distribution of Dufton et al. (2022). This has also been found by Zorec et al. (2016) for their sample of Galactic Be-type stars. Hence a choice of a different sub-sample would not ameliorate this discrepancy.

The above discussion has relied on either a direct or indirect comparison with the grids of models of Brott et al. (2011a). Hence this could be affected by the assumptions made when generating these grids. For example if the adopted calibration for rotational mixing was not appropriate, modest nitrogen enhancement might be possible at higher γ_e-values than implied by Fig. 5. However, recent studies provide no support for a decrease in the efficiency

of rotational mixing and indeed imply that significantly nitrogen enhancements in some apparently single B-type stars would require enhanced rotational mixing (Grin et al. 2017; Dufton et al. 2018; Bouret et al. 2021).

In summary, the estimated nitrogen enhancements may be consistent with a single star sample but encounter several problems, as follows:

(i) The Be-type phenomenon would have to be possible at relatively low γ_e-values, which presents difficulties for theoretical models for generating their discs (Rivinius, Carciofi & Martayan 2013; Hastings, Wang & Langer 2020). However, this would be consistent with the γ_e-distribution found by Dufton et al. (2022) for the VFTS Be-type sample.

(ii) The atmospheric parameters found from the BONNSAI simulations are systematically shifted from our estimated values leading to a suppression in the degree of rotational mixing. Additionally, the distribution of the inclination of the rotational axes from these simulations does not appear to be random.

(iii) The γ_e-distributions implied by the estimated nitrogen abundances and from the de-convolution of projected rotational distributions are in poor agreement, even when biases in the former are considered.

Hence, we conclude that although a single star evolution pathway may account for some Be-type targets, it is unlikely to be the only mechanism responsible for their production.

6.2 Binary evolution

The fraction of Be-type stars that is produced via the binary channel is currently poorly constrained. As discussed in the introduction, it is certainly non-zero, since the binary channel is probably responsible for the OBe-type/X-ray binaries (Reig 2011) and Be-type stars in other systems (Kennea et al. 2021; Wang et al. 2021). In this scenario, the B-type star is spun-up close to critical rotation by accreting matter from a companion. After a stage as sub-dwarf, helium star or Wolf–Rayet star, which typically lasts about 10 per cent of the Be-type star lifetime (Langer et al. 2020a), the companion forms a compact object, i.e. a white-dwarf, neutron star or black hole.

In the Be-type stellar mass range considered here, all three types of compact objects could be companions, although neutron stars are likely to dominate. When a neutron star forms in a Be-type binary, the likelihood that its formation kick breaks up the binary is estimated to be ∼80 per cent (Eldridge, Langer & Tout 2011). However, some of our Be-type targets may be at the post-mass transfer stage with a sub-dwarf, helium star or Wolf–Rayet companion (Langer et al. 2020a; Shao & Li 2021) as suggested, e.g. for the Galactic star, LB1 (Liu et al. 2019; Shenar et al. 2020). Hence if all our Be-type stars were formed in binaries, we would expect a binary fraction of at least 20 per cent and possibly higher.

Dunstall et al. (2015) found only six SB1 candidates for the VFTS Be-type stars. Villaseñor et al. (2021) subsequently undertook additional spectroscopy and identified one SB1 system (#874) and five SB1*systems (#213, 337, 697, 847, and 877), the latter being targets showing clear signs of periodicity but with more tentative periods. Assuming that the rotational period of the primary is synchronized with the orbital period, it is possible to estimate the angle of inclination. In turn, adopting the primary BONNSAI mass estimates discussed above, the secondary mass can be found from the mass functions of Villaseñor et al. (2021). The Roche lobe radii can then be estimated using the methodology of Eggleton (1983) – further details can be found in Dufton et al. (2023). For #697 and #847, these estimates are smaller than the estimated stellar radii, which would imply that there would be no space to accommodate a Be-type disc. We consider that some other mechanism, such as pulsations may be the origin of the reported periodic radial velocity shift. Disregarding these two objects, our analysis provides abundance estimates for the SB1 system (#874)[7] and one SB1*(#213), both of which show no nitrogen enhancement. Their disc contributions (f_c) are 27 and 5 per cent, respectively, consistent with those found for the other targets. This would then imply that the flux contributions from the secondaries are relatively small as these should have manifested themselves as an additional disc contamination.

The orbital periods of Be/X-ray binaries are typically found in the range between 10 and 1000 d, with a peak of the distribution near 100 d (Walter et al. 2015), which agrees well with binary population synthesis predictions (Langer et al. 2020b). For such systems, the radial velocity amplitude of the Be-type star due to the orbital motion would be expected to be smaller than the SB1 detection threshold of Dunstall et al. (2015). Hence, some of our apparently single Be-type stars could have evolved via a binary channel.

Dufton et al. (2022) also searched for evidence of binarity in the VFTS Be-type sample by investigating the dispersion in their radial velocity estimates. They found relatively large standard deviation of the order of 20 km s^{-1} for the whole sample. However by only considering targets in the two older clusters, Hodge 301 and SL 639, and correcting their stellar radial velocities to the rest-frame cluster velocities (Patrick et al. 2019), they found a smaller standard deviation of 3.5 km s^{-1} for the 16 Be-type stars compared to 8.3 km s^{-1}f or the 11 B-type stars. If our Be-type sample contained a significant number of stars that had been in binary system, disrupted by the supernova explosion of their companion, they should exhibit a kick velocity. Renzo et al. (2019) found that these kicks were typically <30 km s^{-1}, although their analysis concentrated on larger mass stars (>15 M$_\odot$). Van den Heuvel et al. (2000) considered systems with lower mass primaries (10 and 12 M$_\odot$) with mass ratios between 0.3 and 0.8. They found kick velocities of 5–22 km s^{-1}. Given the small dispersion in the radial velocity estimates, this pathway would not appear to be significant for this Be-type sub-sample. However, the dispersion would be consistent with either Be-type stars being single or with them currently having low mass evolved companions.

Evolutionary models for rotating single stars predict that the nitrogen surface enhancement will increase with time due to rotational mixing (see Section 6.1). Such a trend is not expected for the binary channel of Be-type stellar formation, where two different mechanisms may contribute. First, before the accretion event, the less massive star that will evolve into a Be-type star may have been subject to rotational mixing, analogous to that of single stars. However, in contrast to Be-type stars originating from the single star channel, which presumably were born as rapid rotators, Be-type stars in binaries probably started their lives as B-type stars with a range of rotational velocities. For the VFTS binary sample, $v_e \sin i$-estimates have been obtained for the confirmed SB1 systems by Garland et al. (2017) and for the SB2 systems by Dufton et al. (2023). These have a median of 110 km s^{-1}, which assuming that their axes of inclination are randomly orientated would translate into a median rotational

[7]The nitrogen abundance in #874 is less than the LMC baseline but we note that both carbon and oxygen appear underabundant, implying that the flux contamination may have been underestimated. Alternatively, it may reflect inadequacies in the adopted methodology as discussed by Ahmed & Sigut (2017) for their sample.

velocity of approximately 140 km s^{-1}. For a 8 M$_\odot$ single star[8] and this initial rotational velocity, BONNSAI predicts a nitrogen enhancement of only 0.2 dex at the end of its main-sequence evolution. However the distribution is asymmetric with a tail of larger v_e sin i-values. For example 24 per cent of the VFTS binary stars have a v_e sin i-estimate >200 km s^{-1}, which would correspond to a nitrogen enhancement of at least 0.6 dex at the end of the hydrogen burning main sequence.

There may be several biases in the binary v_e sin i-distribution adopted here. First, binaries with large angles of inclination may have been preferentially identified due to their large range of radial velocity variations (see e.g. Ramírez-Agudelo et al. 2015). This would manifest itself by too large a median for the v_e sin i-estimates. Secondly, binaries may be preferentially identified with low v_e sin i-values as the narrower metal line spectrum will provide more reliable radial velocity estimates (see e.g. Dunstall et al. 2015). This would manifest itself by too small an estimate of the median v_e sin i-estimate. Finally, the current v_e sin i-estimates may not be appropriate to the evolution of the stellar rotational velocity before an accretion event (Dufton et al. 2023). However, these biases are unlikely to be so large as to vitiate the main implication of the VFTS binary $v_e$sin i-distribution – namely that a significant fraction of the secondary population will have undergone little nitrogen enhancement prior to an accretion event.

The accretion of hydrogen burning products from the the originally more massive donor may also enhance the surface nitrogen abundance of the secondary, i.e. the precursor Be-type star. The amount of nitrogen-rich matter received depends on the accretion history (the most enriched matter would be transferred near the end of the mass transfer phase), and on the accretion efficiency, i.e. the fraction of the transferred mass which is accreted. Conservative mass transfer in models without rotation leads to nitrogen enrichment of 0.3–0.7 dex (Langer 2012). Notably, the enhancement is moderated by thermohaline mixing, which dilutes the accreted enriched material in the whole envelope of the mass gainer (Wellstein, Langer & Braun 2001). By contrast, the nitrogen enhancement in the case of inefficient mass transfer – which is always sufficient to spin-up the mass gainer – is typically only 0.3–0.5 dex, and the Be-type stars in some systems are not enhanced at all (Langer et al. 2020b; Sen et al. 2022).

For the binary channel, the rapid rotation of the recently formed Be-type star does not itself contribute to further surface nitrogen enrichment. The reason is that the Be-type star progenitor during its core hydrogen burning evolution, preferentially in the second half, has developed a substantial H/He-gradient zone above the convective core. The strong mean molecular weight gradient in this zone prevents any mixing of nitrogen from the core to the surface, even after the spin-up of the mass gainer to close-to-critical rotation (Wang et al. 2023).

In summary, the nitrogen enhancement in binary produced Be-type stars should be in the range 0–1 dex, where the rotational mixing before the binary interaction and the accretion of nitrogen-rich matter can both contribute. However, the information about the spin of the Be-type star progenitor is wiped out by the mass transfer process, such that no correlation between rotation and enrichment is expected.

Even though two processes contribute to enrich the binary produced Be-type stars, their enrichment may not be larger than that of Be-type stars produced through single star evolution, because the latter evolve only from the B-type stars born with the largest spins. As discussed in Section 6.1, this pre-selection made Hastings, Wang & Langer (2020) propose that, based on the models of Brott et al. (2011a), Be-type stars from the single star channel in the LMC should have a nitrogen surface abundance of at least $\epsilon_N = 7.7$ dex, corresponding to $\Delta\epsilon_N \geq 0.8$ dex. Given that the nitrogen abundances found in our sample are generally less than this limit, binary evolution is an attractive mechanism for the formation of, at least some, of the Be-type sample. This would also help explain the low nitrogen abundances found in the previous analyses of Galactic Be-type stars by Ahmed & Sigut (2017) and Magellanic Cloud Be-type stars by Dunstall et al. (2011).

7 CONCLUDING REMARKS

The principal results from this analysis of the VFTS Be-type stars are:

(i) Useful nitrogen abundances (or upper limits) could be found for 23 of the sample of 67 VFTS Be-type stars. Reliable estimates could not be found for the remaining targets due to the Si III spectrum not being visible.

(ii) These lead to a range of nitrogen enhancement from 0.0 up to 1.0 dex with a median enhancement of 0.33 dex. These results are consistent with the small nitrogen enrichments in Be-type samples found previously by Dunstall et al. (2011) and Ahmed & Sigut (2017).

(iii) Current single star evolutionary models cannot explain the low nitrogen abundances found in some stars in sample. Any successful theory would require the formation of discs at a relatively low fraction of critical rotation, $\gamma_e \gtrsim 0.4$. Additionally, it would have to reconcile the different γ_e-distributions implied by the deconvolution of the v_e sin i-estimates and those of the nitrogen abundance.

(iv) The number of confirmed binaries is small especially when compared with that found in normal B-type stars. However, the expected radial velocity variations in systems that have undergone mass transfer are small enough that there may be undiscovered binaries in our sample as discussed by Bodensteiner, Shenar & Sana (2020).

(v) A binary evolutionary history with relatively little rotational mixing in the earlier stages and an inefficient mass transfer would be compatible with the low nitrogen abundances found here and elsewhere. However, any quantitative comparison has not been possible given our relatively small sample size and the diversity of evolutionary pathways.

Although our sample of Be-type nitrogen abundances is the largest yet published for the LMC, it suffers from being incomplete. However, it implies that current single star evolutionary models cannot be responsible for the formation of all Be-type stars. Indeed, the investigation of Hastings, Wang & Langer (2020) found that a nitrogen abundance enhancement of at least 0.8 dex should be present. The nitrogen enhancements listed in Table 1 would then imply that 20 targets were incompatible with a single star evolutionary pathway,[9] constituting approximately 30 per cent of the VFTS Be-type sample. As low nitrogen abundances cannot be ruled out for the Be-type stars that were not analysed, this provides an estimate for the lower limit for Be-type stars not formed via a single star pathway. It also provides a lower limit for the percentage of Be-type stars that appear to be formed via binary interactions, assuming that there are no other currently unidentified pathways. This would be consistent with

[8]Given the median mass estimate of approximately 9 M$_\odot$ for our sample, the Be-type star precursors will presumably have been less massive.

[9]Allowing for a possible systematic error due to our adoption of zero microturbulence (see Section 4.1) would only decrease this to 19 targets.

the previous analysis of the $v_e \sin i$-estimates for the VFTS Be-type sample (Dufton et al. 2022), where the observations were easier to reconcile with a binary interaction pathway.

ACKNOWLEDGEMENTS

We are grateful for helpful comments by the referee. Based on observations at the European Southern Observatory Very Large Telescope in programmes 171.D-0237, 182.D-0222, and 096.D-0825. This work has received funding from the European Research Council (ERC) under the European Union's Horizon 2020 research and innovation programme (grant agreement number 945806) and is supported by the Deutsche Forschungsgemeinschaft (DFG, German Research Foundation) under Germany's Excellence Strategy EXC 2181/1-390900948 (the Heidelberg STRUCTURES Excellence Cluster).

DATA AVAILABILITY

The spectroscopic data were obtained during ESO programmes, 171.D-0237171.0237, 182.D-0222, and 096.D-0825. Data products are available from the ESO Science Archive Portal (https://archive.eso.org/scienceportal/home). Spectra are available at http://www.roe.ac.uk/~cje/tarantula/spectra, https://star.pst.qub.ac.uk/~sjs/flames/, or on request from the authors.

REFERENCES

Ahmed A., Sigut T. A. A., 2017, MNRAS, 471, 3398
Bastian N. et al., 2017, MNRAS, 465, 4795
Bodensteiner J., Shenar T., Sana H., 2020, A&A, 641, A42
Bouret J. C., Martins F., Hillier D. J., Marcolino W. L. F., Rocha-Pinto H. J., Georgy C., Lanz T., Hubeny I., 2021, A&A, 647, A134
Brott I. et al., 2011a, A&A, 530, A115
Brott I. et al., 2011b, A&A, 530, A116
De Mink S. E., Langer N., Izzard R. G., Sana H., de Koter A., 2013, ApJ, 764, 166
Doazan V., Franco M., Rusconi L., Sedmak G., Stalio R., 1983, A&A, 128, 171
Dufton P. L., Ryans R. S. I., Trundle C., Lennon D. J., Hubeny I., Lanz T., Allende Prieto C., 2005, A&A, 434, 1125
Dufton P. L. et al., 2018, A&A, 615, A101
Dufton P. L., Evans C. J., Hunter I., Lennon D. J., Schneider F. R. N., 2019, A&A, 626, A50
Dufton P. L., Lennon D. J., Villaseñor J. I., Howarth I. D., Evans C. J., de Mink S. E., Sana H., Taylor W. D., 2022, MNRAS, 512, 3331
Dufton P. L., Langer N., Lennon D. J., Villaseñor J. I., Evans C. J., Sana H., Taylor W. D., 2023, to be submitted
Dunstall P. R., Brott I., Dufton P. L., Lennon D. J., Evans C. J., Smartt S. J., Hunter I., 2011, A&A, 536, A65
Dunstall P. R. et al., 2015, A&A, 580, A93
Eggleton P. P., 1983, ApJ, 268, 368
Eldridge J. J., Langer N., Tout C. A., 2011, MNRAS, 414, 3501
Evans C. J. et al., 2011, A&A, 530, A108
Evans C. J. et al., 2015, A&A, 574, A13
Garland R. et al., 2017, A&A, 603, A91
Garnett D. R., 1999, in Chu Y.-H., Suntzeff N., Hesser J., Bohlender D., eds., IAU Symposium Vol. 190, New Views of the Magellanic Clouds. ASP Technical Publications, San Francisco, p. 266
Gray D. F., 2005, The Observation and Analysis of Stellar Photospheres, 3rd edn. Cambridge Univ. Press, Cambridge
Grin N. J. et al., 2017, A&A, 600, A82
Hastings B., Wang C., Langer N., 2020, A&A, 633, A165
Hastings B., Langer N., Wang C., Schootemeijer A., Milone A. P., 2021, A&A, 653, A144
Hubeny I., 1988, Computer Physics Communications, 52, 103
Hubeny I., Lanz T., 1995, ApJ, 439, 875
Hubeny I., Heap S. R., Lanz T., 1998, in Howarth I.ed., ASP Conf. Ser. Vol. 131, Properties of Hot Luminous Stars. ASP Technical Publications, San Francisco, p. 108
Hunter I. et al., 2007, A&A, 466, 277
Hunter I. et al., 2009, A&A, 496, 841
Jaschek C., Jaschek M., 1990, The Classification of Stars. Cambridge Univ. Press, Cambridge
Kennea J. A., Coe M. J., Evans P. A., Townsend L. J., Campbell Z. A., Udalski A., 2021, MNRAS, 508, 781
Kurt C. M., Dufour R. J., 1998, in Dufour R. J., Torres-Peimbert S., eds, Revista Mexicana de Astronomia y Astrofisica Conference Series Vol. 7, Revista Mexicana de Astronomia y Astrofisica Conference Series. Instituto de Astronomía, Mexico City, p. 202
Langer N., 2012, ARAA, 50, 107
Langer N., Baade D., Bodensteiner J., Greiner J., Rivinius T., Martayan C., Borre C. C., 2020a, A&A, 633, A40
Langer N. et al., 2020b, A&A, 638, A39
Lanz T., Hubeny I., 2007, ApJS, 169, 83
Liu J. et al., 2019, Nature, 575, 618
Martayan C., Hubert A. M., Floquet M., Fabregat J., Frémat Y., Neiner C., Stee P., Zorec J., 2006, A&A, 445, 931
Martayan C., Floquet M., Hubert A. M., Gutiérrez-Soto J., Fabregat J., Neiner C., Mekkas M., 2007, A&A, 472, 577
McEvoy C. M. et al., 2015, A&A, 575, A70
Milone A. P. et al., 2018, MNRAS, 477, 2640
Pasquini L. et al., 2002, The Messenger, 110, 1
Patrick L. R. et al., 2019, A&A, 624, A129
Pols O. R., Cote J., Waters L. B. F. M., Heise J., 1991, A&A, 241, 419
Ramírez-Agudelo O. H. et al., 2015, A&A, 580, A92
Reig P., 2011, Ap&SS, 332, 1
Renzo M. et al., 2019, A&A, 624, A66
Rivinius T., Carciofi A. C., Martayan C., 2013, A&A Rev., 21, 69
Ryans R. S. I., Dufton P. L., Mooney C. J., Rolleston W. R. J., Keenan F. P., Hubeny I., Lanz T., 2003, A&A, 401, 1119
Salpeter E. E., 1955, ApJ, 121, 161
Sana H. et al., 2013, A&A, 550, A107
Schneider F. R. N., Langer N., de Koter A., Brott I., Izzard R. G., Lau H. H. B., 2014, A&A, 570, A66
Schootemeijer A., Lennon D. J., Garcia M., Langer N., Hastings B., Schürmann C., 2022, A&A, 667, A100
Sen K. et al., 2022, A&A, 659, A98
Shao Y., Li X.-D., 2014, ApJ, 796, 37
Shao Y., Li X.-D., 2020, ApJ, 898, 143
Shao Y., Li X.-D., 2021, ApJ, 908, 67
Shenar T. et al., 2020, A&A, 639, L6
Struve O., 1931, ApJ, 73, 94
Telting J. H., Kaper L., 1994, A&A, 284, 515
Thaller M. L., Bagnuolo William G. J., Gies D. R., Penny L. R., 1995, ApJ, 448, 878
Trundle C., Dufton P. L., Hunter I., Evans C. J., Lennon D. J., Smartt S. J., Ryans R. S. I., 2007, A&A, 471, 625
van den Heuvel E. P. J., Rappaport S., 1987, in Slettebak A., Snow T. P.eds, IAU Colloq. 92: Physics of Be Stars. Cambridge Univ. Press, Cambridge, p. 291
van den Heuvel E. P. J., Portegies Zwart S. F., Bhattacharya D., Kaper L., 2000, A&A, 364, 563
Villaseñor J. I. et al., 2021, MNRAS, 507, 5348
Walter R., Lutovinov A. A., Bozzo E., Tsygankov S. S., 2015, A&A Rev., 23, 2
Wang C. et al., 2023, A&A, 670, A43
Wang L., Gies D. R., Peters G. J., Götberg Y., Chojnowski S. D., Lester K. V., Howell S. B., 2021, AJ, 161, 248
Wellstein S., Langer N., Braun H., 2001, A&A, 369, 939
Zorec J., Briot D., 1997, A&A, 318, 443
Zorec J. et al., 2016, A&A, 595, A132

APPENDIX: COMMENTS ON INDIVIDUAL STARS

Below we comment briefly on the analysis for the targets that are listed in Table 1.

#034: The effective temperature estimated from the He II spectrum is 700 K lower than that implied by the spectral type. The significant rotational broadening leads to only three O II lines appearing unblended.

#101: The effective temperature was deduced from the spectral type, although the estimate was consistent with a marginal identification of the He II line at 4686 Å. Due to the large projected rotational velocity, only the strongest Si III line was clearly identified, whilst no other unblended metal lines were observed. The large upper limit on the equivalent width of the N II line led to the upper limit to the nitrogen abundance being poorly constrained.

#135: The combination of significant rotational broadening and a relatively low S/N makes the spectrum difficult to analyse and may explain the relatively large silicon abundance even for zero f_c. Alternatively, it may imply a non-zero microturbulence with $v_t \gtrsim 2\,\mathrm{km\,s^{-1}}$ being consistent with a normal silicon abundance.

#152: The effective temperature estimated from the Si II to Si III ionization equilibrium is 1700 K higher than that implied by the spectral type. Although O II spectrum is weak, it is relatively well observed with five abundance estimates having a standard deviation of ±0.18 dex.

#164: The Si II line at 4553 Å was not measurable due to nearby emission. There was a marginal identification of the N II line at 3995 Å but an upper limit to the equivalent width has been adopted.

#194: The metal line spectrum is well observed, although the nitrogen abundance is an upper limit

#196: The spectrum was relatively poor with the weakest Si III line at 4574 Å not being measurable.

#213: The spectrum is well observed and despite the low nitrogen abundance estimate, the N II line at 3995 Å is clearly present.

#237: The effective temperature was estimated from the Si IV to Si III ionization equilibrium. The Si IV spectrum is weak and the $T_{\rm eff}$ estimate is lower by 2200 K than that deduced from the spectral type. However, it is consistent with the absence of the He II line at 4686 Å, which would have been clearly visible at the higher effective temperature estimate implied by the spectral type. All the other metal lines used in the analysis are well observed, although some of the O II multiplets could not be used due to blending.

#268: The spectrum has a relatively low S/N ratio of ∼75 with the Si III line at 4574 Å not being measurable. The N II line at 3995 Å is clearly visible implying significant nitrogen enrichment.

#283: The metal line spectrum is well observed despite the significant rotational broadening. The small implied silicon abundance could be due to stochastic errors in the equivalent width measurements or in the adopted atmospheric parameters. Alternative a microturbulence with $v_t \gtrsim 1\,\mathrm{km\,s^{-1}}$ would remove the discrepancy.

#293: The effective temperature, estimated using the spectral type, is consistent with the absence of either Si II or Si IV features (see e.g. Dufton et al. 2018). The other metal lines used in the analysis are well observed, although the O II spectrum was weak leading to only two estimates.

#322: The spectrum was relative poor with only the strongest Si III line and C II line at 4267 Å clearly present and the upper limit on the nitrogen abundance being poorly constrained.

#395: The effective temperature estimated from the Si IV to Si III ionization equilibrium is in good agreement with that deduced from the spectral type for a luminosity class III, consistent with the estimated gravity. Evans et al. (2015) identified some cross-fibre contamination from the Wolf–Rayet star, RMC 135 (#402), that prevents the use of the He II spectrum as an additional $T_{\rm eff}$ criterium. The metal line spectrum is well observed.

#683: Despite the large $v_e \sin i$ estimate, the metal line spectrum is relatively well observed. The O II spectrum is present but blending of the strongest features prevents reliable abundance estimates.

#697: The effective temperature estimated from the He II spectrum is 700 K lower than that implied by the spectral type. The metal line spectrum is well observed, although only an upper limit is available for the nitrogen abundance.

#738: The effective temperature estimated from the He II spectrum is 800 K higher than that implied by the spectral type. The metal spectrum is well observed, although that for Mg II is weak consistent with the relatively high effective temperature.

#756: The effective temperature estimated from the He II spectrum is 3000 K lower than that implied by the spectral type. The estimated gravity is low and more consistent with a luminosity class I (see e.g. McEvoy et al. 2015), which would reduce the discrepancy to 1800 K. The Si III multiplet is affected by nearby emission leading to the estimate of the disc contribution, f_c, being poorly constrained. The N II line at 3995 Å is well observed.

#825: The spectroscopy is relatively poor due to the low S/N and the large rotational broadening. The Si III multiplet is clearly seen but implies an overabundance of silicon. The low estimated gravity would be consistent with a non-zero microturbulence, with a value, $v_t \gtrsim 2\,\mathrm{km\,s^{-1}}$ being required to remove this discrepancy. The upper limit to the nitrogen abundance is poorly constrained.

#835: The effective temperature has been estimated from the Si IV to Si III ionization equilibrium. The Si IV spectrum is weak and the $T_{\rm eff}$ estimate is lower by 1300 K than that deduced from the spectral type. However, it is consistent with the absence of the He II line at 4686 Å, which should have been visible at the higher effective temperature estimate. The metal spectrum is well observed with, e.g. the oxygen abundance estimates from 10 lines having a standard deviation of ±0.18 dex.

#847: The spectroscopy is relatively poor due to the large rotational broadening. The Si III multiplet is clearly seen but implies an overabundance of silicon. The low estimated gravity would be consistent with a non-zero microturbulence, with a value, $v_t \gtrsim 2\,\mathrm{km\,s^{-1}}$ being required to remove this discrepancy. The only other metal line that could be measured was that of N II at 3995 Å.

#848: The metal line spectrum was relatively well observed, although the Si III line at 4553 Å was affected by emission. There was a marginal identification of the N II line at 3995 Å but an upper limit to equivalent width has been adopted.

#874: The effective temperature was estimated using the spectral type and is consistent with the absence of either Si II or Si IV features (see e.g. Dufton et al. 2018). The Mg II line at 4481 Å could not be used as it appeared to be contaminated by an emission feature. A modest underabundance of ∼0.2 dex is found for carbon, nitrogen, and oxygen and may reflect uncertainties in the flux contamination or the adoption of zero microturbulence.

This paper has been typeset from a TEX/LATEX file prepared by the author.